Modeling and Control of a Bifilar Crane Payload

Andrej Cibicik[1], Torstein A. Myhre[1] and Olav Egeland[1]

***Abstract*— This paper presents a modeling technique and a controller for an underactuated crane payload. The crane payload is modeled as a bifilar pendulum. The payload is attached to a sheave block, such that a cable can freely run to either side. This configuration is often used in different types of cranes, including offshore cranes. To achieve asymptotic stability in the absence of damping, we propose a controller based on an energy approach and the passivity properties of the system. We prove stability of the system with the proposed controller using LaSalle's invariance principle.**
The control performance is studied in the numerical simulations. The simulation results show that all the states of the closed-loop system with coupled sway and skew dynamics converge to the origin.

I. INTRODUCTION

Cranes are used in various hoisting operations both onshore and offshore. The motion of the crane and external forces, such as waves and wind, induce payload oscillations. The motion of the payload can be classified into sway oscillations and torsional oscillations. The torsional oscillations are also referred to as skew motion in recent publications ([1], [2], [3], [4]). The growth of both types of oscillations causes great risk for the safety of personnel and other equipment. In order to facilitate safe and efficient crane operations several researchers have focused on the control of the sway and skew motion of crane payloads. In this paper we model the payload as a bifilar pendulum and derive a control law for the sway and skew motion.

A mass suspended by two cables is known as a bifilar pendulum. In 1967 Kane derived a full nonlinear dynamical model of a bifilar pendulum [5]. Similar bifilar or extended four-cabled pendulum models are used for the dynamic modeling of crane payloads. In practice a payload is often suspended by two cables running through a sheave block or a spreader with the sheaves attached to the payload, see Fig. 1. This bifilar arrangement allows for a lower capacity winch, which reduces the cost of the crane. The field of dynamics and control of cranes with a payload is well-presented in the review paper [6]. A typical assumption in the literature is that the bifilar pendulum can be modeled as a simple spherical pendulum with a lumped mass, which means that the skew dynamics are not included. Based on [6], it can be concluded that the research on crane payloads modeled as a simple spherical pendulum is dominating in the field. However, in [7] the authors model a planar Maryland Rigging system and derive a control law for the sway motion. A Maryland Rigging system is a crane payload configuration

[1] The authors are with the Dept. of Mechanical and Industrial Engineering, Norwegian University of Science and Technology, NO-7465 Trondheim, Norway. andrej.cibicik@ntnu.no

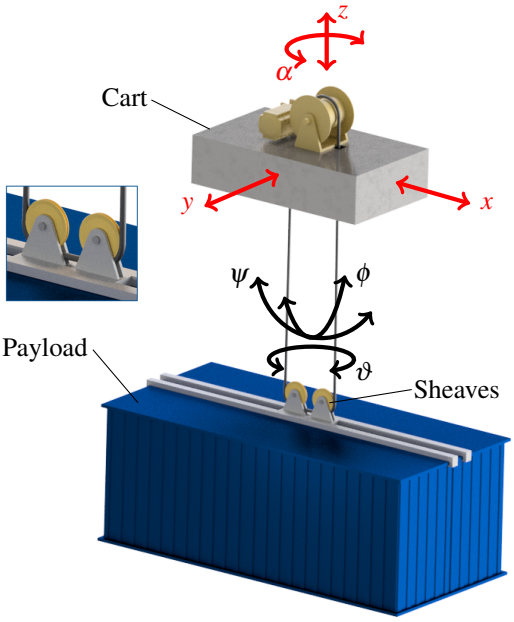

Fig. 1. An underactuated bifilar cart-payload system. A spreader with sheaves is rigidly attached to the payload. The red arrows indicate actuated DOFs and the black arrows indicate unactuated DOFs.

where the payload is modeled as a double pendulum. The top pendulum is bifilar with a sheave at the bottom end of the cable as in Fig. 1. The lower pendulum in this system is planar or spherical. In such configuration the length of each cable is dependent on the payload sway angle (see [7]). Control of the spatial sway motion of the lumped mass in a Maryland Rigging configuration is investigated in [8]. Another configuration of a bifilar payload with parallel cables is presented in [9] and [10], where the authors model the skew dynamics and derive a controller for the skew motion, using a skew actuator device located in the spreader. In [1] a similar actuator device in the spreader (as in [9]) for a bifilar payload with parallel cables is modeled. The authors derive a controller for skew orientation adjustment during the container hoisting operations in harbours. An alternative crane configuration is a container gantry crane with a payload suspended by four cables. This system is dynamically similar to a bifilar pendulum. The importance of the skew and sway motion coupling for container crane systems is highlighted in [11] and [12], where the authors derive a kinematic and dynamical model of the container crane payload. A model-based PID controller for the container crane payload is presented in [13] and a fuzzy control strategy for the similar configuration is presented in [2]. An input shaping technique

for controlling the skew motion, based on the 3D dynamics of the payload, is proposed in [3] and [14]. The authors utilize a separate actuator to control the length of each of the four cables. A gantry crane with two carts, each hoisting one end of the container, for the simultaneous sway and skew control is presented in [4].

An energy-based approach is often used for the control of pendulums or other underactuated systems. Often researchers use this approach for the stabilization of a pendulum at the unstable equilibria, for example [15], [16], [17], [18]. Alternatively, a passivity-based controller minimizing the oscillations around the stable equilibria of a planar pendulum is presented in [19]. In [20] several passivity-based controllers that asymptotically regulate the planar gantry position and the payload angle are derived. In the field of robotics an energy-based control approach is used for asymptotic stabilization of robotic manipulators with flexible joints [21], [22]. It might not be obvious, but a mathematical model of a manipulator link with a flexible joint is similar to the one of a pendulum attached to an actuated cart. The link motor resembles the cart (actuated part), while the link itself resembles the pendulum (unactuated part). The flexible spring element in the joint has the same role as an equivalent spring stiffness of the pendulum due to the displacement from the vertical position. Flexible joint manipulators are discussed in [21] and [22], where the authors derive simple PD controllers with gravity compensation for a manipulator with flexible joints. The derived controller only needs feedback from the motor to asymptotically stabilize the link about the desired position.

As it has been discussed in [1], [9] and [10], for some applications of the bifilar payload configuration it is important to consider the skew dynamics. In the case when there is a demand for faster hoisting operations, a moving crane will also induce the sway motion of the payload. A control problem of such combined sway and skew motion has been highlighted and discussed for the container payloads suspended by the four cables [11], [12]. However, to the best of our knowledge, this problem for the bifilar payload configuration has not been discussed in the literature before. Therefore, we want to address the control problem of the combined sway and skew motion for a bifilar payload configuration.

In this paper we present a mathematical model of the cart-payload system, where the payload is modeled as a bifilar pendulum. The physical payload configuration is similar to the upper pendulum of the Maryland rigging system [7], where a cable can run over the sheave. We consider a case when a sheave block is attached to the payload (Fig. 1). Additionally, we include the skew dynamics, which is modeled based on the method proposed in [9]. We also present an energy-based control law asymptotically stabilizing the origin of the system. The derived PD controller with gravity compensation only needs a feedback input from the cart.

This paper is organized as follows. In Section II the model assumptions, kinematic and dynamical modeling of the system are presented. In Section III we present derivation

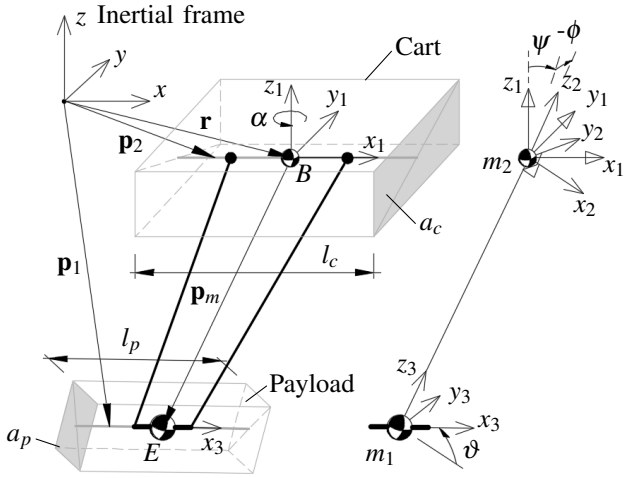

Fig. 2. To the left: The origin of Frame 1 is attached at the center of gravity (CoG) of the cart . The origin of Frame 3 is attached at the CoG of the payload. Both frames follow motion of the bodies. To the right: the spherical sway of the payload is given by the angles ϕ and ψ. The skew rotation of the payload is given by the angle ϑ.

of the control law and the stability proof. In Section IV we show the results of the numerical simulations and in Section V we provide the conclusions.

II. Dynamic modelling

In the first part of this section the kinematics of the system is defined. Then the dynamical equations of motion are derived using the Euler-Lagrange equation.

A. Kinematic modeling

As shown in Fig. 2 and 3, the crane system consists of two bodies: a gantry crane cart and a crane payload with the sheaves attached. The cable goes down from the cart towards the payload, where it bends around the sheaves and then goes back to the cart, where it is anchored. The sheave block is rigidly attached to the payload.

The payload can be modeled as a rectangular beam with the cross-sectional area a_p and the length l_p. The center of gravity (CoG) of the payload is located in the point E (Fig. 2). The cart can also be modeled as a rectangular beam with the cross-sectional area a_c and the length l_c. The CoG of the cart is located in the point B (Fig. 2).

The position of the CoG of the cart is described by three orthogonal translations, given by the coordinate vector $\mathbf{r} \in \mathbb{R}^3$. The orientation of the cart is described by the rotation angle α about the z axis. The motion of the payload is described by the sway angles: ψ about the y_1 axis, ϕ about the x_2 axis and the skew angle ϑ about the z_2 axis. The following coordinate frames are used in the model: the fixed inertial frame is defined as Frame 0, the cart fixed body frame is Frame 1, the intermediate frame rotated by ϕ and ψ from the cart fixed body frame is Frame 2 and the payload fixed body frame is Frame 3. The rotation matrix from Frame 0

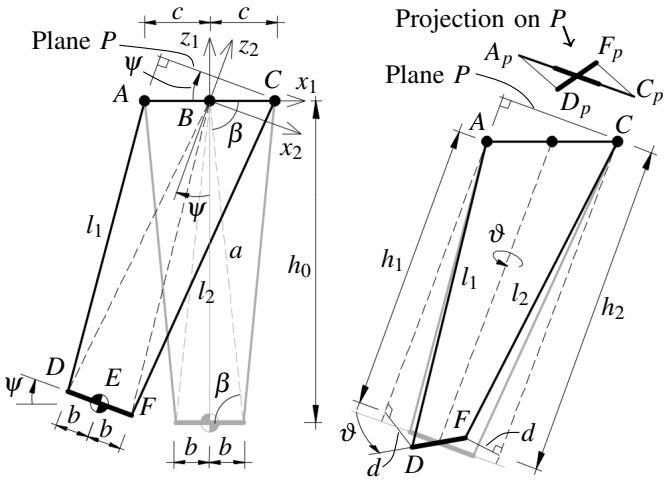

(a) The initial rest position is shown in grey. The rotation about the y_1 axis by the angle ψ brings the system to the position shown in black, note that now $l_1 < l_2$.

(b) The initial ψ-displaced position is shown in grey. An additional rotation about the z_2 axis by the angle ϑ brings the system to the position shown in black.

Fig. 3. Kinematic definitions

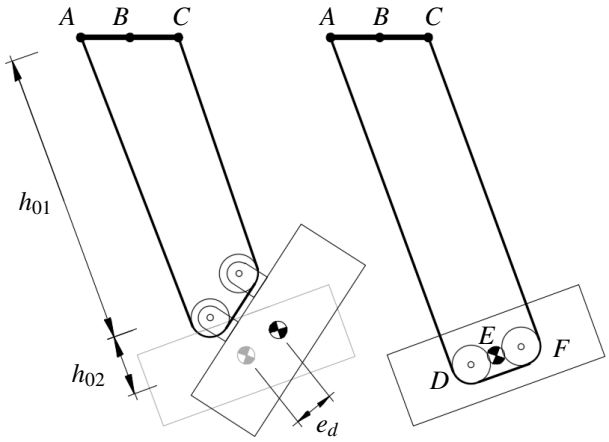

Fig. 4. A displacement e_d caused by the rotation of the payload is negligible when $h_{01} \gg h_{02}$, as the global x,y,z position of the payload is still described with sufficient accuracy. The CoG of the payload is assumed to be located between the sheaves in the point E.

to Frame 1 is given by

$$\mathbf{R}_r = \mathbf{R}_1^0(\alpha) = \mathbf{R}_z(\alpha). \tag{1}$$

The rotation matrix from Frame 1 to Frame 2 is given by

$$\mathbf{R}_2^1(\phi,\psi) = \mathbf{R}_y(\psi)\mathbf{R}_x(\phi). \tag{2}$$

The rotation matrix from Frame 1 to Frame 3 is given by

$$\mathbf{R}_\theta = \mathbf{R}_3^1(\boldsymbol{\theta}) = \mathbf{R}_y(\psi)\mathbf{R}_x(\phi)\mathbf{R}_z(\vartheta). \tag{3}$$

The matrices $\mathbf{R}_x(\cdot)$, $\mathbf{R}_y(\cdot)$ and $\mathbf{R}_z(\cdot)$ are the orthogonal rotation matrices about the x, y and z axes respectively.
The position of the CoG of the cart is given in the inertial frame as

$$\mathbf{r} = \begin{bmatrix} x & y & z \end{bmatrix}^{\mathrm{T}}. \tag{4}$$

The vector of pendulum rotations is given by

$$\boldsymbol{\theta} = \begin{bmatrix} \phi & \psi & \vartheta \end{bmatrix}^{\mathrm{T}}. \tag{5}$$

The total vector of generalized coordinates is then given by

$$\mathbf{q} = \begin{bmatrix} \boldsymbol{\theta}^{\mathrm{T}} & \mathbf{r}^{\mathrm{T}} & \alpha \end{bmatrix}^{\mathrm{T}}. \tag{6}$$

In practice the crane will not be operated under the conditions where the sway or the skew becomes too large, as this may cause damage to the payload or risk of personnel injury. Therefore, a reasonable domain of interest for $\boldsymbol{\theta}$ could be limited to $D_\theta = \{\boldsymbol{\theta} \in \mathbb{T}^3 |\ |\phi| \le \frac{\pi}{6}, |\psi| \le \frac{\pi}{6}, |\vartheta| \le \frac{\pi}{2}\}$, where $\mathbb{T}^3 = S^1 \times S^1 \times S^1$ is a Cartesian product of three circles.

The spatial position of an arbitrary point on the payload in the inertial frame is given by

$$\mathbf{p}_1 = \mathbf{r} + \mathbf{R}_r(\mathbf{p}_m^1 + \mathbf{R}_\theta \mathbf{p}_{01}^3), \tag{7}$$

where the vector $\mathbf{p}_{01}^3$ defines the position of an arbitrary point on the payload with respect to the payload CoG in Frame 3.

The spatial position of an arbitrary point on the cart in the inertial frame is given by

$$\mathbf{p}_2 = \mathbf{r} + \mathbf{R}_r \mathbf{p}_{02}^1, \tag{8}$$

where the vector $\mathbf{p}_{02}^1$ defines the position of an arbitrary point on the cart with respect to the cart CoG in Frame 1.

An exact mathematical model of a bifilar pendulum with a sheave block could be rather complicated as it involves modeling of the contact between the sheaves and the cable. We propose a simplified model which is defined in a compact matrix form, such that it is convenient to apply Lyapunov's stability theory for the design of an energy-based controller. The assumptions in the derived model are based on the discussion in the next paragraph.

As the sheave block is mechanically a hinge, an additional payload rotation about the sheave block is possible (Fig. 4). When the length of the cable h_{01} is much larger than the distance h_{02}, then the global displacement e_d caused by the additional payload rotation will be relatively small, compared to the displacement due to the sway. We can simplify the equations of motion significantly by neglecting this payload rotation, while the global position of the payload is still described with sufficient accuracy. The assumption is implemented by assuming that the payload always remains perpendicular to the line BE (Fig. 4). Furthermore, the CoG of the payload is assumed to be located between the sheaves in the point E (Fig. 4). The list of the other assumptions is presented below.

- If the pendulum is rotated by the angle ψ in the x_1z_1 plane (Fig. 3(a)), then the exact geometrical path of the point E is an ellipse. However, when the focal length of an ellipse AC is smaller than the minor semi-axis h_0, then for the small ψ values the elliptical path can be quite accurately represented by a circle;
- When a cable runs over a sheave, the length of each cable in the bifilar pendulum is different (Fig. 3). We assume that both cables are attached to the sheave and

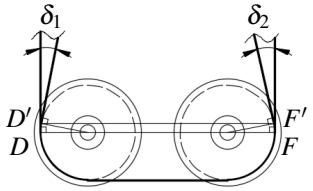

Fig. 5. The variation of the distance DF due to δ_i angles is neglected, as it is minor and has no significant influence on the dynamics.

the length of each cable l_1, l_2 is given by the function of ψ;

- In Fig. 5 the distance $DF = 2b$ is dependent on at which angle the cable leaves the sheave. The variation is assumed insignificant for the small sway angles. Therefore, for any value of the angles δ_1 and δ_2 it is assumed that $DF = D'F' = 2b$, where b is defined in Fig. 3(a).

For the notations in the following derivations we refer to Fig. 3. The distance $a = BD = BF$ is given by

$$a = \sqrt{h_0^2 + b^2}. \tag{9}$$

The angle β is given by

$$\beta = \arctan\frac{h_0}{b}. \tag{10}$$

The cable lengths are given by the cosine rule as

$$\begin{aligned} l_1^2 &= a^2 + c^2 - 2ac\cos(\beta - \psi), \\ l_2^2 &= a^2 + c^2 - 2ac\cos(\beta + \psi). \end{aligned} \tag{11}$$

The plane P (Fig. 3) is always normal to z_2 axis (or, in the other words, parallel to the x_3y_3 plane). The projection of c on the plane P is given by

$$c_p = \cos(\psi)c. \tag{12}$$

The cable projections on the plane P are given by

$$d^2 = b^2 + c_p^2 - 2bc_p\cos(\vartheta). \tag{13}$$

The height projections of the skewed cables are given by

$$h_1 = \sqrt{l_1^2 - d^2}, \quad h_2 = \sqrt{l_2^2 - d^2}. \tag{14}$$

The mean of the h_i values gives the distance from the point B to the payload CoG

$$h = 0.5(h_1 + h_2). \tag{15}$$

Then the position of the payload CoG is expressed in Frame 2 by

$$\mathbf{p}_m^2(\boldsymbol{\theta}) = \begin{bmatrix} 0 & 0 & -h \end{bmatrix}^{\mathrm{T}}. \tag{16}$$

Note that a superscript $(\cdot)^2$ in $\mathbf{p}_m^2$ denotes that coordinates are given in Frame 2. The vector $\mathbf{p}_m^2$ can be transformed to Frame 1 by

$$\mathbf{p}_m^1(\boldsymbol{\theta}) = \mathbf{R}_2^1\mathbf{p}_m^2. \tag{17}$$

Note that if $\boldsymbol{\theta} = \mathbf{0}$, then $\mathbf{p}_m^1(\mathbf{0}) = \begin{bmatrix} 0 & 0 & -h_0 \end{bmatrix}^{\mathrm{T}}$.

B. Differential kinematics and equations of motion

Both sway and skew motion contribute to the kinetic energy in the system. The governing source of kinetic energy of the skew motion is the rotation ϑ. The linear velocity of the payload along $\mathbf{p}_m$ due to the skew motion is relatively small and the kinetic energy of that motion can be neglected. The same assumption was made by the authors in [1] and [9]. Mathematically this can be implemented by assuming

$$\mathbf{p}_m^2(\boldsymbol{\theta}) \simeq \tilde{\mathbf{p}}_m^2 = \begin{bmatrix} 0 & 0 & -h_0 \end{bmatrix}^{\mathrm{T}}, \tag{18}$$

and

$$\tilde{\mathbf{p}}_m^1(\boldsymbol{\theta}) = \mathbf{R}_2^1\tilde{\mathbf{p}}_m^2. \tag{19}$$

Note that this assumption is only used for the calculation of the kinetic energy. The potential energy is calculated using the expressions given by (16) and (17).
The velocity of an arbitrary point on the payload is derived by differentiation of (7) with respect to time

$$\dot{\mathbf{p}}_1(\mathbf{q}, \dot{\mathbf{q}}) = \dot{\mathbf{r}} + \mathbf{R}_r(\mathbf{P} + \mathbf{B})\dot{\boldsymbol{\theta}} + \mathbf{B}_r(\tilde{\mathbf{p}}_m^1 + \mathbf{R}_\theta\mathbf{p}_{01}^3)\dot{\alpha}, \tag{20}$$

where the new matrix notations are introduced as

$$\mathbf{P} = \frac{\partial\tilde{\mathbf{p}}_m^1}{\partial\boldsymbol{\theta}}, \quad \mathbf{B} = \frac{\partial(\mathbf{R}_\theta\mathbf{p}_{01}^3)}{\partial\boldsymbol{\theta}}, \quad \mathbf{B}_r = \frac{\partial\mathbf{R}_r}{\partial\alpha}. \tag{21}$$

The velocity of an arbitrary point on the cart is derived by differentiation of (8) with respect to time.

$$\dot{\mathbf{p}}_2(\mathbf{q}, \dot{\mathbf{q}}) = \dot{\mathbf{r}} + \mathbf{B}_r\mathbf{p}_{02}^1\dot{\alpha}. \tag{22}$$

Equation (20) can be written in the matrix form as

$$\dot{\mathbf{p}}_1 = \begin{bmatrix} \mathbf{L} & \mathbf{I} & \mathbf{N} \end{bmatrix}\dot{\mathbf{q}}, \tag{23}$$

where the matrices $\mathbf{L}$ and $\mathbf{N}$ are defined as

$$\mathbf{L} = \mathbf{R}_r(\mathbf{P} + \mathbf{B}), \quad \mathbf{N} = \mathbf{B}_r(\tilde{\mathbf{p}}_m^1 + \mathbf{R}_\theta\mathbf{p}_{01}^3) \tag{24}$$

and $\mathbf{I}$ is the identity matrix.
Equation (22) can be written in the matrix form as

$$\dot{\mathbf{p}}_2 = \begin{bmatrix} \mathbf{0} & \mathbf{I} & \mathbf{H} \end{bmatrix}\dot{\mathbf{q}}, \tag{25}$$

where the matrix $\mathbf{H}$ is defined as

$$\mathbf{H} = \mathbf{B}_r\mathbf{p}_{02}^1. \tag{26}$$

For the sake of simplicity the payload and the cart are modeled as a slender rod. The mass of the cable is relatively small and is neglected. The mass of the payload m_1 is uniformly distributed along the x_3 axis. The mass of the cart m_2 is uniformly distributed along the x_1 axis. The rotational inertia of the payload about the x_3 axis and the rotational inertia of the cart about the x_1 axis is equal to zero. In the case when this inertia is significant it is straightforward to extend the presented procedure for a 2D or 3D body representation. As the payload is a slender rod, then $\mathbf{p}_{01}^3 = [x_3\ 0\ 0]^{\mathrm{T}}$. This leads to $\mathbf{R}_\theta\mathbf{p}_{01}^3 = \mathbf{R}_\theta^{\langle 1\rangle}x_3$ and the matrix $\mathbf{B}$ from (21) can be simplified to

$$\mathbf{B} = \bar{\mathbf{B}}x_3 = \begin{bmatrix} \frac{\partial\mathbf{R}_\theta^{\langle 1\rangle}}{\partial\phi} & \frac{\partial\mathbf{R}_\theta^{\langle 1\rangle}}{\partial\psi} & \frac{\partial\mathbf{R}_\theta^{\langle 1\rangle}}{\partial\vartheta} \end{bmatrix} x_3, \tag{27}$$

where the operator $(\cdot)^{\langle i \rangle}$ defines the i-th column of a matrix. As the cart is also modeled as a slender rod, then $\mathbf{p}_{02}^1 = [x_1 \ 0 \ 0]^{\mathrm{T}}$ and the matrix $\mathbf{H}$ from (26) is simplified to

$$\mathbf{H} = \mathbf{B}_r^{\langle 1 \rangle} x_1. \tag{28}$$

The kinetic energy of the payload is given by

$$\mathscr{T}_1 = \frac{1}{2}\rho_p \int_{V_1} \dot{\mathbf{p}}_1^{\mathrm{T}} \dot{\mathbf{p}}_1 \, dV_1 = \frac{1}{2}\dot{\mathbf{q}}^{\mathrm{T}} \mathbf{M}_1 \dot{\mathbf{q}}, \tag{29}$$

where ρ_p is the payload material density and

$$\mathbf{M}_1 = \rho_p a_p \int_{-0.5l_p}^{0.5l_p} \begin{bmatrix} \mathbf{L}^{\mathrm{T}}\mathbf{L} & \mathbf{L}^{\mathrm{T}} & \mathbf{L}^{\mathrm{T}}\mathbf{N} \\ \mathbf{L} & \mathbf{I} & \mathbf{N} \\ \mathbf{N}^{\mathrm{T}}\mathbf{L} & \mathbf{N}^{\mathrm{T}} & \mathbf{N}^{\mathrm{T}}\mathbf{N} \end{bmatrix} dx_3. \tag{30}$$

The kinetic energy of the cart is given by

$$\mathscr{T}_2 = \frac{1}{2}\rho_c \int_{V_2} \dot{\mathbf{p}}_2^{\mathrm{T}} \dot{\mathbf{p}}_2 \, dV_2 = \frac{1}{2}\dot{\mathbf{q}}^{\mathrm{T}} \mathbf{M}_2 \dot{\mathbf{q}}, \tag{31}$$

where ρ_c is the cart material density and

$$\mathbf{M}_2 = \rho_c a_c \int_{-0.5l_c}^{0.5l_c} \begin{bmatrix} \mathbf{0} & \mathbf{0} & \mathbf{0} \\ \mathbf{0} & \mathbf{I} & \mathbf{H} \\ \mathbf{0} & \mathbf{H}^{\mathrm{T}} & \mathbf{H}^{\mathrm{T}}\mathbf{H} \end{bmatrix} dx_1. \tag{32}$$

The potential energy of the payload is given by

$$\mathscr{V}_1 = m_1 g \mathbf{e}_3 (\mathbf{r} + \mathbf{R}_r \mathbf{p}_m^1) = m_1 g \mathbf{e}_3 (\mathbf{r} + \mathbf{p}_m^1), \tag{33}$$

where $\mathbf{e}_3 = \begin{bmatrix} 0 & 0 & 1 \end{bmatrix}$. Pre-multiplication of a column vector with $\mathbf{e}_3$ returns the last element of the column vector.
The potential energy of the cart is given by

$$\mathscr{V}_2 = m_2 g \mathbf{e}_3 \mathbf{r}. \tag{34}$$

The total kinetic, potential energy and the Lagrangian of the system are given by

$$\mathscr{T} = \sum_{i=1}^{2} \mathscr{T}_i, \quad \mathscr{V} = \sum_{i=1}^{2} \mathscr{V}_i, \quad \mathscr{L} = \mathscr{T} - \mathscr{V}. \tag{35}$$

The Euler-Lagrange equation of motion is

$$\frac{d}{dt}\left(\frac{\partial \mathscr{L}}{\partial \dot{\mathbf{q}}}\right)^{\mathrm{T}} - \left(\frac{\partial \mathscr{L}}{\partial \mathbf{q}}\right)^{\mathrm{T}} = \boldsymbol{\tau}, \tag{36}$$

where $\boldsymbol{\tau}$ is the vector of input forces. By substitution of (35) into (36) and performing derivations we get the equations of motion, which are written as

$$\mathbf{M}(\mathbf{q})\ddot{\mathbf{q}} + \mathbf{C}(\mathbf{q}, \dot{\mathbf{q}})\dot{\mathbf{q}} + \mathbf{G}(\mathbf{q}) = \boldsymbol{\tau}, \tag{37}$$

where $\mathbf{M}(\mathbf{q}) = \mathbf{M}_1 + \mathbf{M}_2$, and the elements $C_{i,j}$ of $\mathbf{C}$ are given by

$$C_{ij} = \sum_k \frac{\partial M_{ij}}{\partial q_k}\dot{q}_k - \frac{1}{2}\frac{\partial M_{kj}}{\partial q_i}\dot{q}_k. \tag{38}$$

The vector of conservative gravitational forces is given by

$$\mathbf{G}(\mathbf{q}) = \left(\frac{\partial \mathscr{V}}{\partial \mathbf{q}}\right)^{\mathrm{T}}. \tag{39}$$

The vector of input forces is given by

$$\boldsymbol{\tau} = \begin{bmatrix} 0 & 0 & 0 & \tau_1 & \tau_2 & \tau_3 & \tau_4 \end{bmatrix}^{\mathrm{T}} = \begin{bmatrix} \mathbf{0}^{\mathrm{T}} & \boldsymbol{\tau}_a^{\mathrm{T}} \end{bmatrix}^{\mathrm{T}}. \tag{40}$$

Note that only 4 of 7 states are actuated, so the system is said to be an underactuated dynamical system.

III. Energy-based control

In this section we derive a controller using Lyapunov's direct method. The controller takes the form of a PD controller with gravity compensation.

A. Controller design

The control task is to make the origin of the closed-loop system an asymptotically stable (AS) equilibrium point.

The vector of generalized coordinates is partitioned into actuated and unactuated parts as

$$\mathbf{q} = \begin{bmatrix} \mathbf{q}_u^{\mathrm{T}} & \mathbf{q}_a^{\mathrm{T}} \end{bmatrix}^{\mathrm{T}}, \tag{41}$$

where

$$\mathbf{q}_u = \boldsymbol{\theta}, \quad \mathbf{q}_a = \begin{bmatrix} \mathbf{r}^{\mathrm{T}} & \alpha \end{bmatrix}^{\mathrm{T}}. \tag{42}$$

The mass matrix and the matrix $\mathbf{C}$ are partitioned accordingly

$$\mathbf{M} = \begin{bmatrix} \mathbf{M}_{uu} & \mathbf{M}_{ua} \\ \mathbf{M}_{au} & \mathbf{M}_{aa} \end{bmatrix}, \quad \mathbf{C} = \begin{bmatrix} \mathbf{C}_{uu} & \mathbf{C}_{ua} \\ \mathbf{C}_{au} & \mathbf{C}_{aa} \end{bmatrix}, \tag{43}$$

where $\mathbf{M}_{au} = \mathbf{M}_{ua}^{\mathrm{T}}$. The vector of gravity forces is partitioned as

$$\mathbf{G} = \begin{bmatrix} \mathbf{G}_u^{\mathrm{T}} & \mathbf{G}_a^{\mathrm{T}} \end{bmatrix}^{\mathrm{T}}, \tag{44}$$

where the vector $\mathbf{G}_u$ has the property $\mathbf{G}_u(\mathbf{0}) = \mathbf{0}$ and the vector $\mathbf{G}_a$ is constant and is given by

$$\mathbf{G}_a = \begin{bmatrix} 0 & 0 & g(m_1 + m_2) & 0 \end{bmatrix}^{\mathrm{T}}. \tag{45}$$

We choose a Lyapunov function candidate (LFC) in the form

$$V(\mathbf{q}, \dot{\mathbf{q}}) = \mathscr{T} + \frac{1}{2}k_P \mathbf{q}_a^{\mathrm{T}} \mathbf{q}_a + \mathscr{V}_u, \tag{46}$$

where k_P is a positive constant and $\mathscr{T}$ is defined by (35). The function $\mathscr{V}_u$ is the potential energy of the pendulum due to the displacement from the equilibrium, it is defined as

$$\mathscr{V}_u(\mathbf{q}_u) = m_1 g(\mathbf{e}_3 \mathbf{p}_m^1 + h_0), \tag{47}$$

where $\mathbf{e}_3 = \begin{bmatrix} 0 & 0 & 1 \end{bmatrix}$. From (16) and (17) we get that $\mathbf{e}_3 \mathbf{p}_m^1(\mathbf{0}) = -h_0$. For $\mathbf{q}_u \in D_\theta$, where $D_\theta = \{\mathbf{q}_u \in \mathbb{T}^3 | \ |\phi| \leq \frac{\pi}{6}, |\psi| \leq \frac{\pi}{6}, |\vartheta| \leq \frac{\pi}{2}\}$, the function $\mathbf{e}_3 \mathbf{p}_m^1(\mathbf{q}_u) = -h > -h_0 \ \forall \mathbf{q}_u \neq \mathbf{0}$. This shows that the function $\mathscr{V}_u$ is positive definite. Consequently, the LFC is a positive definite function with a defined minimum at the origin. As for the control of flexible-joint manipulators in [22] the LFC is composed of three components: the total kinetic energy of the system, the re-shaped potential energy of the actuated part, and the potential energy of the unactuated part.

Substitution of (35) and (47) into (46) gives

$$V = \frac{1}{2}\dot{\mathbf{q}}^{\mathrm{T}} \mathbf{M} \dot{\mathbf{q}} + \frac{1}{2}k_P \mathbf{q}_a^{\mathrm{T}} \mathbf{q}_a + m_1 g(\mathbf{e}_3 \mathbf{p}_m^1 + h_0). \tag{48}$$

The time derivative of V along the trajectories of (37) is

$$\dot{V} = \dot{\mathbf{q}}^{\mathrm{T}} \mathbf{M} \ddot{\mathbf{q}} + \frac{1}{2}\dot{\mathbf{q}}^{\mathrm{T}} \dot{\mathbf{M}} \dot{\mathbf{q}} + k_P \dot{\mathbf{q}}_a^{\mathrm{T}} \mathbf{q}_a + \dot{\mathbf{q}}_u^{\mathrm{T}} \mathbf{G}_u, \tag{49}$$

where

$$\frac{d\mathscr{V}_u}{dt} = \frac{\partial \mathscr{V}_u}{\partial \mathbf{q}_u}\dot{\mathbf{q}}_u = \dot{\mathbf{q}}_u^{\mathrm{T}} \mathbf{G}_u, \tag{50}$$

given that from (33), (34), (35) and (47) we obtain

$$\frac{\partial \mathscr{V}_u}{\partial \mathbf{q}_u} = \frac{\partial \mathscr{V}}{\partial \mathbf{q}_u}. \tag{51}$$

Substitution of $\mathbf{M}\ddot{\mathbf{q}}$ from (37) into (49) leads to

$$\dot{V} = \dot{\mathbf{q}}^{\mathrm{T}}(-\mathbf{C}\dot{\mathbf{q}} - \mathbf{G} + \boldsymbol{\tau}) + \frac{1}{2}\dot{\mathbf{q}}^{\mathrm{T}}\dot{\mathbf{M}}\dot{\mathbf{q}} + k_P\dot{\mathbf{q}}_a^{\mathrm{T}}\mathbf{q}_a + \dot{\mathbf{q}}_u^{\mathrm{T}}\mathbf{G}_u. \tag{52}$$

Using the skew-symmetric property of the matrix $(\dot{\mathbf{M}} - 2\mathbf{C})$, (52) is simplified to

$$\dot{V} = \dot{\mathbf{q}}^{\mathrm{T}}(-\mathbf{G} + \boldsymbol{\tau}) + k_P\dot{\mathbf{q}}_a^{\mathrm{T}}\mathbf{q}_a + \dot{\mathbf{q}}_u^{\mathrm{T}}\mathbf{G}_u. \tag{53}$$

From (39), (41) and (44) it follows that

$$\dot{\mathbf{q}}_a^{\mathrm{T}}\mathbf{G}_a = \dot{\mathbf{q}}^{\mathrm{T}}\mathbf{G} - \dot{\mathbf{q}}_u^{\mathrm{T}}\mathbf{G}_u \tag{54}$$

and from (40) and (41) it follows that

$$\dot{\mathbf{q}}^{\mathrm{T}}\boldsymbol{\tau} = \dot{\mathbf{q}}_a^{\mathrm{T}}\boldsymbol{\tau}_a. \tag{55}$$

By substitution of (54) and (55) into (53) we get

$$\dot{V} = \dot{\mathbf{q}}_a^{\mathrm{T}}(-\mathbf{G}_a + \boldsymbol{\tau}_a + k_P\mathbf{q}_a). \tag{56}$$

The control input $\boldsymbol{\tau}_a$ is chosen such that

$$-\mathbf{G}_a + \boldsymbol{\tau}_a + k_P\mathbf{q}_a = -k_D\dot{\mathbf{q}}_a, \tag{57}$$

where k_D is a positive constant. By substitution of (57) into (56) we get

$$\dot{V} = -k_D\dot{\mathbf{q}}_a^{\mathrm{T}}\dot{\mathbf{q}}_a \leq 0. \tag{58}$$

Equation (58) shows that the time derivative of the Lyapunov function is negative semi-definite, thus the origin of the closed-loop system is a stable equilibrium point. From (57) the control input is expressed in the form of a PD controller with gravity compensation

$$\boldsymbol{\tau}_a = -k_D\dot{\mathbf{q}}_a - k_P\mathbf{q}_a + \mathbf{G}_a. \tag{59}$$

From (58) it follows that the inequality $V \leq V(t=0)$ holds. That is the upper bound on V depends on the initial conditions. From (46) it is noted that if V is upper bounded, then $(\mathscr{T} + \mathscr{V}_u)$ and $\mathbf{q}_a$ are upper bounded.

B. Stability analysis

Asymptotic stability of the origin of the closed-loop system is now proven using LaSalle's invariance principle and Corollary 4.1 in [23].

Theorem 1: Define $D = \{\mathbf{q} \in \mathbb{R}^7 \mid \mathbf{q}_u \in D_\theta\}$. Let $\Omega \subset D$ be a compact bounded positively invariant set with respect to (37) with the control law (59) and let the origin be the only equilibrium point in D. Then every solution of the closed-loop system (37), (59) started in Ω will approach the origin as $t \to \infty$.

Proof: Define a compact positively invariant bounded set Ω such that $\Omega = \{D \mid V(\mathbf{q}, \dot{\mathbf{q}}) \leq V(t=0)\}$. Define S such that $S = \{\Omega \mid \dot{V}(\mathbf{q}, \dot{\mathbf{q}}) = 0\}$.

From (58) it follows that $\dot{\mathbf{q}}_a = 0$ in S, consequently $\ddot{\mathbf{q}}_a = 0$ and $\mathbf{q}_a = \tilde{\mathbf{q}}_a$, where $\tilde{\mathbf{q}}_a$ is a constant.

Provided that $\dot{\mathbf{q}}_a = 0$, $\mathbf{q}_a = \tilde{\mathbf{q}}_a$ and $\mathbf{G}_a$ are constants, from (59) it follows that the input $\boldsymbol{\tau}_a = -k_P\tilde{\mathbf{q}}_a + \mathbf{G}_a$ is constant in S. The force $\mathbf{G}_a$ (45) is a constant vertical force, which exactly compensates the gravity force.

Assume that $\tilde{\mathbf{q}}_a \neq 0$ in S, then from (59) $\tau_{ai} \neq 0$ for $i = 1,2,4$ and $\tau_{ai} \neq G_{ai}$ for $i = 3$, which leads to a contradiction, as a constant input will result in the motion of the cart. If the cart moves, then $\dot{\mathbf{q}}_a \neq 0$ and a solution trajectory leaves S. Hence, the only case when a solution trajectory remains in S is $\tilde{\mathbf{q}}_a = 0$.

We use the result $\mathbf{q}_a = 0, \dot{\mathbf{q}}_a = 0, \ddot{\mathbf{q}}_a = 0$ and substitute the values into (37). Then the first three equations of the system in S are written in the matrix form as

$$\mathbf{M}_{uu}(\mathbf{q}_u)\ddot{\mathbf{q}}_u + \mathbf{C}_{uu}(\mathbf{q}_u, \dot{\mathbf{q}}_u)\dot{\mathbf{q}}_u + \mathbf{G}_u(\mathbf{q}_u) = 0 \tag{60}$$

and the last four equations are written in the matrix form as

$$\mathbf{M}_{au}(\mathbf{q}_u)\ddot{\mathbf{q}}_u + \mathbf{C}_{au}(\mathbf{q}_u, \dot{\mathbf{q}}_u)\dot{\mathbf{q}}_u = 0. \tag{61}$$

One can verify that the same equation as (60) can be derived by following the procedure from Section II for a single-mass system consisting of a bifilar pendulum without a cart and without any nonconservative forces. This way it can be shown that (60) has the properties: $\mathbf{M}_{uu}$ is a symmetric, positive definite matrix and the matrix $(\dot{\mathbf{M}}_{uu} - 2\mathbf{C}_{uu})$ is skew-symmetric. Stability properties of (60) are analyzed using Lyapunov's direct method. We select the LFC as

$$V_1(\mathbf{q}_u, \dot{\mathbf{q}}_u) = \frac{1}{2}\dot{\mathbf{q}}_u^{\mathrm{T}}\mathbf{M}_{\mathbf{uu}}\dot{\mathbf{q}}_u + \mathscr{V}_u, \tag{62}$$

where $\mathscr{V}_u$ is given by (47). The derivative of (62) with respect to time along the trajectories of (60) is

$$\dot{V}_1 = \dot{\mathbf{q}}_u^{\mathrm{T}}(\mathbf{M}_{\mathbf{uu}}\ddot{\mathbf{q}}_u + \frac{1}{2}\dot{\mathbf{M}}_{\mathbf{uu}}\dot{\mathbf{q}}_u + \mathbf{G}_u). \tag{63}$$

Substitution of $\mathbf{M}_{uu}\ddot{\mathbf{q}}_u$ from (60) into (63) and using the skew-symmetric property of the matrix $(\dot{\mathbf{M}}_{uu} - 2\mathbf{C}_{uu})$ leads to

$$\dot{V}_1 = 0. \tag{64}$$

Equation (64) shows that the system (60) is conservative, so the solutions of (60), started outside the equilibria, will be periodic.

The system of all equations in (60), (61) will have a nontrivial solution only if the solutions of (60) are also the solutions of (61) and vice versa.

The first row of (61) can be explicitly written as

$$\begin{aligned} -\cos(\psi)\ddot{\psi} + \sin(\psi)\dot{\psi}^2 &= 0, \\ For \quad 0 < \psi \leq \frac{\pi}{6}&: \ \ddot{\psi} = k_1\dot{\psi}^2, \\ For \ -\frac{\pi}{6} \leq \psi < 0&: \ \ddot{\psi} = -k_2\dot{\psi}^2, \end{aligned} \tag{65}$$

where $k_1, k_2 > 0$. One can verify that the solution of (65) is nonperiodic, thus it is not a solution of (60). Consequently the only solution satisfying both (60) and (65) is $\psi(t) \equiv 0$. Now we substitute this result into the second row of (61) and after the derivation we obtain

$$\begin{aligned} \cos(\phi)\ddot{\phi} - \sin(\phi)\dot{\phi}^2 &= 0, \\ For \quad 0 < \phi \leq \frac{\pi}{6}&: \ \ddot{\phi} = k_3\dot{\phi}^2, \\ For \ -\frac{\pi}{6} \leq \phi < 0&: \ \ddot{\phi} = -k_4\dot{\phi}^2, \end{aligned} \tag{66}$$

where $k_3, k_4 > 0$. As the solution of (66) is also nonperiodic, thus it is not a solution of (60). Consequently the only solution satisfying both (60) and (66) is $\phi(t) \equiv 0$. Now we substitute this and the previous results into the fourth row of (61) and after the derivation we obtain

$$\ddot{\vartheta} = 0. \tag{67}$$

The solution of (67) is nonperiodic, thus it is not a solution of (60). Consequently, the only solution satisfying both (60) and (67) is $\vartheta(t) \equiv 0$.

From the conclusions followed by (64), (65), (66) and (67) the only solution of the closed-loop system that can stay identically in S is a trivial solution. Thus the solution trajectories of the closed loop system (37), (59) approach the origin as $t \to \infty$.

■

IV. Simulation Results

In this section the performance of the closed-loop system (37), (59) is studied in the simulations. The results for two cases with different system parameters are presented.

A. Simulation Case I

In the first simulation case the load is initially displaced by the angles $\phi = 0.16$ rad and $\psi = -0.24$ rad. Note that no initial skew rotation is applied, however the sway motion eventually excites the skew motion. The other system parameters are given in Table I. The simulation results without active control (when $k_P = 0$, $k_D = 0$) are presented in Fig. 6. The simulation results of the closed-loop system with $k_P = 1400$, $k_D = 7000$ are presented in Fig. 7. The simulation results show fast convergence to the origin of all the states of the system with active control.

TABLE I
System constants for Case I

Constant	h_0	b	c	m_1	m_2	l_p	l_c
Value	10 m	0.25 m	1.0 m	10 t	1.0 t	2.0 m	2.0 m

B. Simulation Case II

In the second simulation case the load is also initially displaced by the angles $\phi = 0.16$ rad and $\psi = -0.24$ rad. The only difference from Case I is that the payload rotational inertia is much larger (note that $l_p = 6.0$ m). The other system parameters are given in Table II. The simulation results of the closed-loop system with $k_P = 1200$, $k_D = 9000$ are presented in Fig. 8. The simulation results show fast convergence to the origin of the sway states and slower convergence of the skew states of the system with active control. This behavior is reasonable taking into account that the skew stiffness is relatively low.

TABLE II
System constants for Case II

Constant	h_0	b	c	m_1	m_2	l_p	l_c
Value	10 m	0.25 m	1.0 m	10 t	1.0 t	6.0 m	2.0 m

The simulation results demonstrate fast convergence of the sway states in both simulations with active control. In Case II, where the rotational inertia of the payload is larger, convergence of the skew states takes longer time. A larger distance between the cables (parameters b, c) would increase the skew stiffness in the system. This way the convergence time for Case II could be improved. To support the conclusions, the simulation results for Case II with the larger cable distance and $k_P = 1200$, $k_D = 9000$ are given in Fig. 9. The payload is again initially displaced by the angles $\phi = 0.16$ rad and $\psi = -0.24$ rad. The only difference from Case II and the data given in Table II is that $b = 2.5$ m and $c = 5.0$ m. As expected, the skew angle ϑ converges to zero faster compared to the results in Fig. 8.

V. Conclusion

We have derived a simplified mathematical model of a bifilar pendulum with a sheave block and we have derived an energy-based controller, which asymptotically stabilizes the origin of the system. A Lyapunov function was chosen based on the system kinetic and potential energy, such that it has a defined minimum at the origin. The stability analysis was based on the LaSalle's invariance principle and Corollary 4.1 in [23]. We have proven that all the states of the closed-loop system approach the origin as the time goes to infinity.

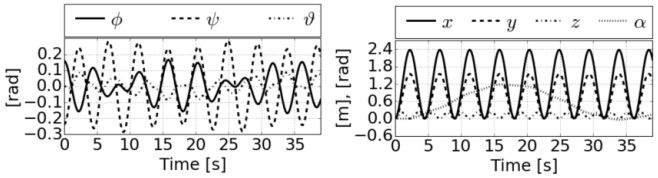

Fig. 6. Simulation results for Case I without active control ($k_P = 0$, $k_D = 0$). The pendulum is displaced by initial conditions $\phi = 0.16$ rad and $\psi = -0.24$ rad. The sway motion excites the skew motion ϑ and all the system states continue to oscillate.

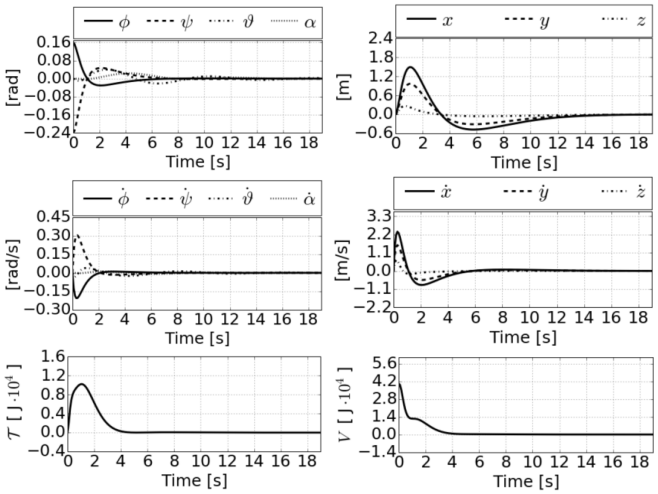

Fig. 7. Simulation results for Case I with $k_P = 1400$ and $k_D = 7000$. The pendulum is displaced by initial conditions $\phi = 0.16$ rad and $\psi = -0.24$ rad. The skew motion ϑ is excited by the sway motion, however the proposed controller ensures fast convergence of all states. The system kinetic energy $\mathcal{T}$ and the value of the Lyapunov function V converge to zero.

We presented simulation results for two different cases. The results showed fast convergence to the origin for the payload with relatively low rotational inertia (Case I). Fast convergence of sway states was also observed in the case of the payload with larger rotational inertia (Case II), however convergence of the skew state took longer time. If fast sway and skew convergence is demanded for the payloads with larger rotational inertia, then the skew stiffness should be increased by increasing the distance between the cables.

A similarity between the presented system and a robotic manipulator with flexible joints was noted. As in the manipulator case, the derived PD controller only required the feedback input from the actuated part and ensured convergence of all states. This similarity can give an indication on which control methods can be applied for solving the tracking problem.

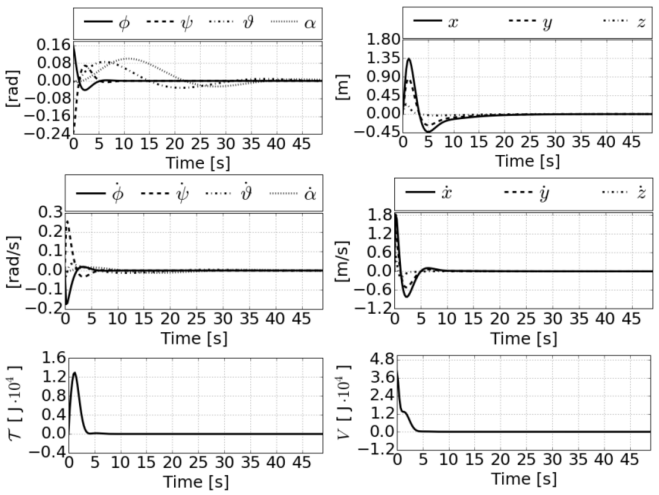

Fig. 8. Simulation results for Case II with $k_P = 1200$ and $k_D = 9000$. The pendulum is displaced by initial conditions $\phi = 0.16$ rad and $\psi = -0.24$ rad. The skew motion ϑ is excited by the sway motion. The proposed controller ensures fast convergence of sway states and slower convergence of the skew states. The system kinetic energy $\mathscr{T}$ and the value of the Lyapunov function V converge to zero.

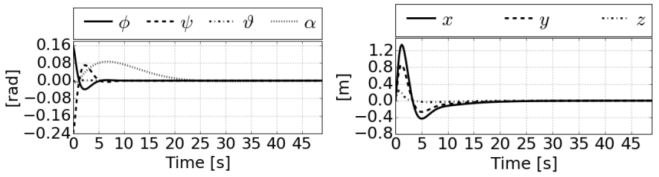

Fig. 9. Simulation results for Case II with the larger cable distance and $k_P = 1200$ and $k_D = 9000$. The pendulum is displaced by initial conditions $\phi = 0.16$ rad and $\psi = -0.24$ rad. Compared to the results in Fig. 8, larger distance between the cables gives faster convergence of the skew states.

ACKNOWLEDGMENT

The research presented in this paper has received funding from the Norwegian Research Council, SFI Offshore Mechatronics, project number 237896.

REFERENCES

[1] U. Schaper, C. Dittrich, E. Arnold, K. Schneider, and O. Sawodny, "2-dof skew control of boom cranes including state estimation and reference trajectory generation," *Control Engineering Practice*, vol. 33, pp. 63–75, 2014.

[2] J.-W. Lee, D.-H. Kim, and K.-T. Park, "Fuzzy control of sway and skew of a spreader by using four auxiliary cables," in *Proceedings of the International Conference on Control, Automation, and Systems*, 2005, pp. 1723–1728.

[3] Q. H. Ngo and K.-S. Hong, "Skew control of a quay container crane," *Journal of Mechanical Science and Technology*, vol. 23, no. 12, pp. 3332–3339, 2009.

[4] G. Smid, J. Klaassens, H. van Nauta Lemke, A. El Azzouzi, and R. Van Der Wekken, "Automatic skew control on container transhipment cranes," *IFAC Proceedings Volumes*, vol. 33, no. 26, pp. 977–982, 2000.

[5] T. Kane and G.-T. Tseng, "Dynamics of the bifilar pendulum," *International Journal of Mechanical Sciences*, vol. 9, no. 2, pp. 83–96, 1967.

[6] E. M. Abdel-Rahman, A. H. Nayfeh, and Z. N. Masoud, "Dynamics and control of cranes: A review," *Journal of Vibration and control*, vol. 9, no. 7, pp. 863–908, 2003.

[7] B. Kimiaghalam, A. Homaifar, M. Bikdash, and B. R. Hunt, "Feedforward control law for a shipboard crane with maryland rigging system," *Modal Analysis*, vol. 8, no. 2, pp. 159–188, 2002.

[8] E. Abdel-Rahman and A. H. Nayfeh, "Two-dimensional control for ship-mounted cranes: a feasibility study," *Modal Analysis*, vol. 9, no. 12, pp. 1327–1342, 2003.

[9] T. Gustafsson, "Modelling and control of rotary crane systems," *PhD thesis*, 1993.

[10] O. Sawodny, A. Hildebrandt, and K. Schneider, "Control design for the rotation of crane loads for boom cranes," in *Proceedings of the IEEE International Conference on Robotics and Automation.*, vol. 2. IEEE, 2003, pp. 2182–2187.

[11] L. Morrish, M. Cartmell, and A. Taylor, "Geometry and kinematics of multicable spreader lifting gear," *Proceedings of the Institution of Mechanical Engineers, Part C: Journal of Mechanical Engineering Science*, vol. 211, no. 3, pp. 185–194, 1997.

[12] M. Cartmell, L. Morrish, and A. Taylor, "Dynamics of spreader motion in a gantry crane," *Proceedings of the Institution of Mechanical Engineers, Part C: Journal of Mechanical Engineering Science*, vol. 212, no. 2, pp. 85–105, 1998.

[13] D. Kim and J. Lee, "Model-based PID control of a crane spreader by four auxiliary cables," *Proceedings of the Institution of Mechanical Engineers, Part C: Journal of Mechanical Engineering Science*, vol. 220, no. 8, pp. 1151–1165, 2006.

[14] Q. H. Ngo, K.-S. Hong, K. H. Kim, Y. J. Shin, and S.-H. Choi, "Skew control of a container crane," in *International Conference on Control, Automation and Systems.* IEEE, 2008, pp. 1490–1494.

[15] K. J. Åström and K. Furuta, "Swinging up a pendulum by energy control," *Automatica*, vol. 36, no. 2, pp. 287–295, 2000.

[16] M. W. Spong, "The swing up control problem for the acrobot," *IEEE control systems*, vol. 15, no. 1, pp. 49–55, 1995.

[17] A. Shiriaev, H. Ludvigsen, O. Egeland, and A. Pogromsky, "On global properties of passivity based control of the inverted pendulum," in *Proceedings of the 38th IEEE Conference on Decision and Control.*, vol. 3. IEEE, 1999, pp. 2513–2518.

[18] W. Zhong and H. Rock, "Energy and passivity based control of the double inverted pendulum on a cart," in *Proceedings of the IEEE International Conference on Control Applications (CCA'01).* IEEE, 2001, pp. 896–901.

[19] J. Collado, R. Lozano, and I. Fantoni, "Control of convey-crane based on passivity," in *Proceedings of the 2000 American Control Conference.*, vol. 2. IEEE, 2000, pp. 1260–1264.

[20] Y. Fang, W. Dixon, D. Dawson, and E. Zergeroglu, "Nonlinear coupling control laws for an underactuated overhead crane system," *IEEE/ASME transactions on mechatronics*, vol. 8, no. 3, pp. 418–423, 2003.

[21] P. Tomei, "A simple PD controller for robots with elastic joints," *IEEE Transactions on automatic control*, vol. 36, no. 10, pp. 1208–1213, 1991.

[22] A. De Luca, B. Siciliano, and L. Zollo, "PD control with on-line gravity compensation for robots with elastic joints: Theory and experiments," *Automatica*, vol. 41, no. 10, pp. 1809–1819, 2005.

[23] H. K. Khalil, *Nonlinear systems*. Pearson Education Limited, 2002, vol. 750.